COMPDYN 2011
III ECCOMAS Thematic Conference on
Computational Methods in Structural Dynamics and Earthquake Engineering
M. Papadrakakis, M. Fragiadakis, V. Plevris (eds.)
Corfu, Greece, 25–28 May 2011

A NUMERICAL STUDY ON THE BEHAVIOR OF HIGH-PERFORMANCE BUCKLING-RESTRAINED BRACES

Tsutomu Usami[1], **Chunlin Wang**[2], **and Jyunki Funayama**[3]

[1] Department of Civil Engineering, Meijo University
1-501 Tempaku-ku, Nagoya, 468-8502, Japan
e-mail: usamit@meijo-u.ac.jp

[2] Department of Civil Engineering, Meijo University
1-501 Tempaku-ku, Nagoya, 468-8502, Japan
e-mail: wangmeijo@gmail.com

[3] Department of Civil Engineering, Meijo University
1-501 Tempaku-ku, Nagoya, 468-8502, Japan
e-mail: 103437009@ccalumni.meijo-u.ac.jp

Keywords: Analytical Study, Buckling-restrained Braces, Steel Bridges, Low-cycle Fatigue.

Abstract. *The paper presents experimental and analytical studies on developing high-performance (i.e., high-energy absorption) BRBs for steel bridge structures. Low-cycle fatigue tests of four BRB's specimens with different constant strain amplitudes and with different constraints on the core brace were conducted as benchmark experiments in order to evaluate the results of the simulations. Both half and whole models of beam elements are proposed with and without taking into account the symmetry of the brace member. Experimental and analytical results show that the BRB's specimens with the stoppers possess better low-cycle fatigue performance than the specimens without the stoppers. The CID performance of steel BRBs with the stoppers even under the strain amplitude, larger than 3%, can meet the requirements of High-performance BRBs but the CID performance of steel BRBs without the stoppers cannot meet the requirements of High-performance BRBs. The friction coefficient of 0.075 is regarded as the right value for the simulations and half and models can effectively simulate the mechanical behavior of the BRB with or without the stoppers.*

1 INTRODUCTION

In the last few decades, the recent trend of seismic design methodology for steel building structures is that the primary members of building structures almost remain elastic and most of the inelastic deformations are enforced to occur in some energy absorption members, such as bracing members. Residual deformations of building structures after a severe earthquake could be reduced based on this design philosophy because most of main members have not been damaged during the earthquake excitation.

This design philosophy has been gradually implemented and refined in steel bridge structures. Developing a reliable method of designing the energy absorption equipment is indispensable. One way is to utilize some lateral or diagonal bracing members in a bridge structure as energy absorption members. Members in the lateral bracing system will be performed under cyclic compression and tension so that they should have high energy absorption capacity. Therefore, in order to obtain a stable performance, the global buckling of bracing members must be restrained by restraining cover members. This is the buckling-restrained brace (BRB), which attracts more and more attentions, because it does not buckle in compression but yield in both tension and compression and represents an effective energy absorption mechanism for damping of engineering structures with low cost.

As an axial-type damping device, BRBs are widely studied on component behavior and system applications in building [1, 2] and bridge engineering [3]. Test results in references[4, 5] show that BRBs process good cumulative inelastic ductility capacity before failure of the core segment, larger than the minimum required value of 200 by AISC seismic provisions[6]. It has been indicated from recent research series by the authors[3, 7] that light weight BRBs were employed to replace insufficient lateral braces and cross diagonal braces for retrofitting an existing steel arch bridge, which leads to damage concentration in sacrificing damping devices and mitigates damage of main structures.

Based on authors' past researches, the concept of high-performance BRBs (HPBRBs) is proposed that no replacement is needed during the lifecycle of bridges and it is likely to suffer three times of strong earthquakes without severe damage[8]. Therefore, besides general performance requirements for BRBs used in building engineering, additional special performance requirements for HPSDs in bridge engineering are summarized as follows [8]: (1) Stable hysteretic characteristics and high energy dissipation capacity; (2) High deformation capacity; (3) High low-cycle fatigue strength; (4) Easy fabrication and construction with low cost; (5) High durability; (6) No need of replacement. Moreover, two performance indices for high-performance BRBs under strong earthquake excitations, the target maximum strain and cumulative inelastic strain, are recommended as 3% and 70%, respectively.

In order to meet the requirements of HPBRBs, series of low-cycle fatigue tests are performed to evaluate the light-weight bolt-assembled steel BRBs proposed by authors[9, 10]. During the experiment, the constraints of the flat core brace, such as the stopper pins used to prevent the relative displacement between the core brace and the restraining members, attracted our attentions and obviously affected the low-cycle fatigue performance verified by the contrastive low-cycle fatigue tests.

In this paper, the experiment, including four steel BRB's specimens looked as the benchmark tests, is firstly presented. These specimens are selected from a series of low-cycle fatigue tests[11] and used to validate both half and whole models of beam elements, considered with and without taking into account the symmetry of the brace member. Details of the experimental and analytical results are given as follows. All the tests were performed at the Advanced Research Center for Seismic Experiments and Computations (ARCSEC) at Meijo University.

2 TEST SPECIMENS AND PROGRAM

As shown in Figure 1, light-weight steel BRBs mainly consist of a steel plate brace member (BM), a pair of restraining members (RMs) connected by high-strength bolts through two filler members, and unbonding material stuck to the brace member as the isolation material in order to reduce the friction between the BM and RMs.

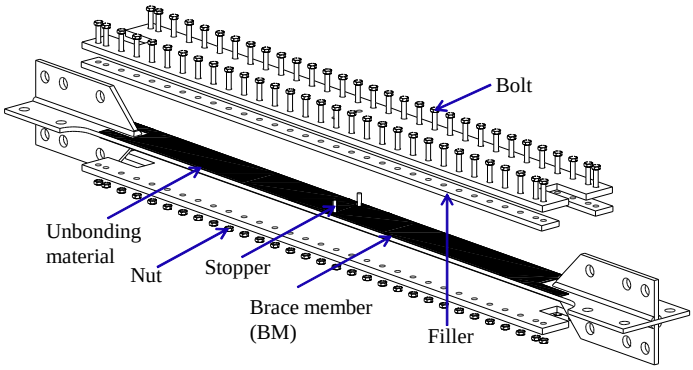

Figure 1: Assemblage of steel BRBs.

2.1 Brace member

The full view of the BM is shown in Figure 2, geometric dimensions and structural properties are listed in Table 1. A flat steel plate is used as the BM, and aiming at well connection to the test equipment, cruciform sections at both ends are expanded by welding 12mm thick rib stiffeners to each side of the plate. The BM is made of SM400A mild steel. Three JIS No.1-typed test pieces for each series are made from the same steel of the BM and average values tested as material constants are listed in Table 2, respectively. At the center of FE-4.0 and FT-3.5 specimens' BMs, two welded stoppers of 9 mm in diameter and 30 mm in height are used to prevent the relative movement between the BM and RMs in the longitudinal direction. But there are nothing at the center of FT-3.5(NS) and FT-4.0(NS) specimens.

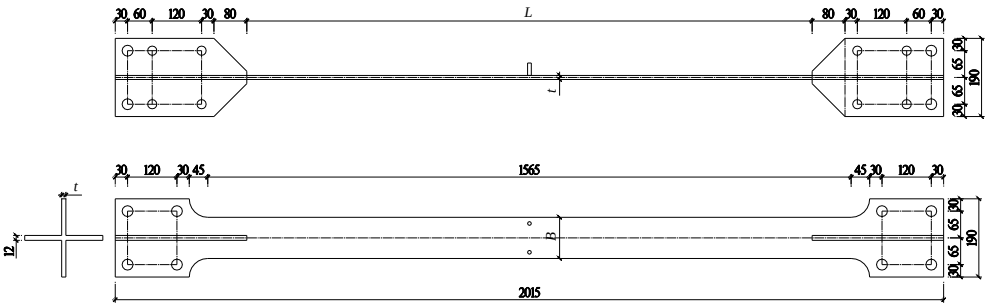

Figure 2: Dimensions of brace member.

Series	Specimen	Steel Type	L	B	t	A(mm^2)	λ	δ_y	Stopper
S-I	FE-4.0	SM400A	1375	99.8	10.3	1028	457	1.91	Yes
S-II	FT-3.5			100.2	10.6	1060	438	1.91	Yes
	FT-3.5(NS)			100.3	10.2	1026	461	1.91	No
	FT-4.0(NS)			100.0	10.6	1060	438	1.91	No

Note: L = length of brace member without cruciform part; B = width; t = thickness; A = sectional area; λ = slenderness ratio on weak axis; P_y = yield axial load; δ_y = Nominal axial yield displacement. Unit: mm.

Table 1: Geometric dimensions and structural properties of BMs.

2.2 Restraining member

Figure 3 gives cross-sectional details of the BRB. The BM is sandwiched by a pair of RMs, and small gaps, d and d_0, are provided between the BM and RMs or filler members. Geometric dimensions and structural properties of RMs are listed in Table 3. The same SM400A mild steel is used for RMs and filler members made of flat steel plates. Nominal values of gap widths are given in Table 3, together with measured material properties of RMs.

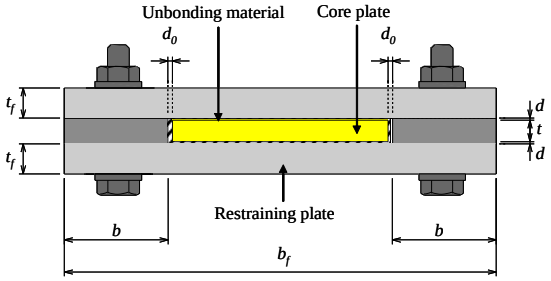

Figure 3: Cross-sectional details of BRB.

Series	Steel Type	E (GPa)	σ_y (Mpa)	ε_y (%)	σ_u (Mpa)	ε_u (%)	ν
S-I	SM400A	210	291	0.139	433	30.2	0.285
S-II		209	251	0.130	409	29.2	0.280

Note: E = Young's modulus; σ_y = yield stress; ε_y =yield strain; σ_u =tensile strength; ν =Poisson ratio.

Table 2: Material constants of brace members.

Series	Steel Type	E^R (Gpa)	σ_y^R (Mpa)	b_f (mm)	t_f (mm)	Gap width (mm)	
						d	d_0
S-I	SM400A	198	260	201	14.3	1	2
S-II		212	264	201	14.3	1	2

Note: E^R=Young's modulus; σ_y^R =yield stress; Notations of b_f, t_f, d and d_0 refer to Figure 3.

Table 3: Geometric dimensions and structural properties of restraining members.

2.3 Testing setup

As shown in Figure 4, the specimen is horizontally pinned by high-strength bolts between two rigid pillars while the BM is horizontally placed. The loading is applied by two jacks parallelly arranged in the vertical direction. The edge of specimens is well treated to avoid eccentric axis load. Before installing specimens, the initial deflection of the specimen is measured in the direction perpendicular to the plate plane so that the initial deflection could direct downward. During a typical experiment, axial displacements of the restrained yielding segment were monitored using eight displacement gauges. These gauges were mounted on both ends of the specimen and displacements were collected by a digital data acquisition system.

2.4 Loading patterns

In the present study, a tensile and compressive alternative cyclic loading controlled by the axial strain of specimens is illustrated in Figure 5. Two cycles of the axial loading of the yield strain amplitude are firstly imposed as an evaluated procedure for testing the specimen and system. For this reason, counting of the cycles starts subsequently. As shown in Figure 5, the constant strain amplitude specified in Table 4 is imposed cyclically until the failure of the BM in the tests. When the loading displacement becomes steady, the strain control equals to the

displacement control. Therefore, we conducted the present fatigue tests by controlling the axial displacement.

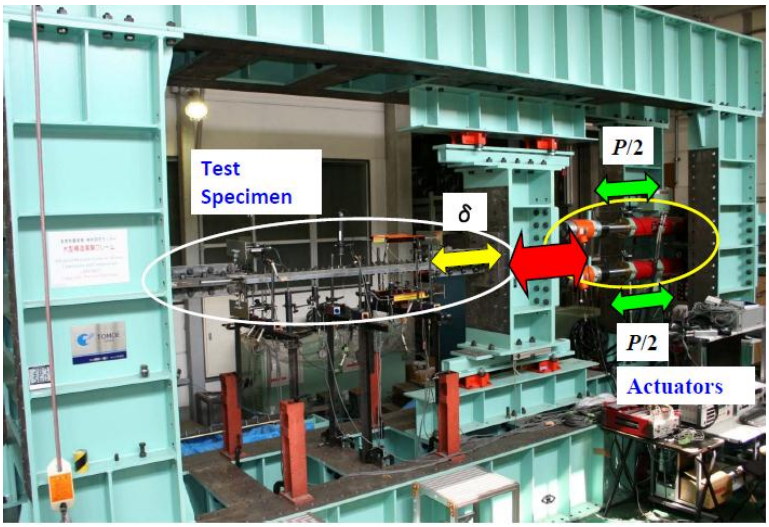

Figure 4: Testing setup

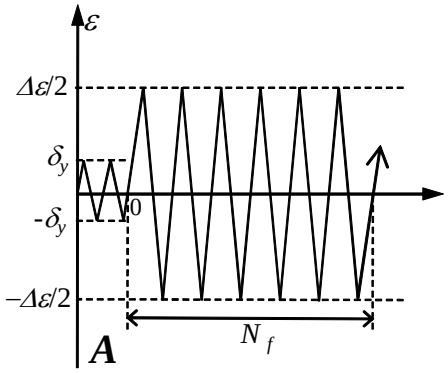

Figure 5: Strain-controlled loading pattern

Series	Test specimen	$\Delta\varepsilon/2$	$\Delta\varepsilon$	$\Delta\varepsilon_e$	$\Delta\varepsilon_p$	N_f	*CID*	Failure position
S-I	FE-4.0	0.040	0.08	0.006	0.074	7	0.96	Mid-span
	FT-3.5	0.035	0.07	0.005	0.065	9	1.18	Mid-span
S-II	FT-3.5(NS)	0.035	0.07	0.005	0.065	5	0.65	Mid-span
	FT-4.0(NS)	0.040	0.08	0.006	0.074	4	0.59	Mid-span

Note: $\Delta\varepsilon/2$ = strain amplitude; $\Delta\varepsilon$ =strain range; $\Delta\varepsilon_e$ = elastic strain range; $\Delta\varepsilon_p$ = plastic strain range; N_f = number of failure cycles; *CID* = cumulative inelastic deformation.

Table 4: Test results of BRB's specimens.

3 TEST RESULTS

3.1 Experimental stress-strain relations

Overall experimental stress-strain curves of the BRBs' specimens are given in Figure 6. The tensile state of BRBs is displayed in the positive direction. The abscissa is the engineering strain, ε, defined as the relative displacement divided by the original length of both ends of the core plate, while the ordinate is the engineering stress, σ, defined as the axial force di-

vided by the original cross-sectional area of the core plate. The core plate indicates the portion of the BM where it behaves plastically. Test results of all the specimens are summarized in Table 4. In addition, stable stress-strain curves were obtained without overall buckling occurrence in the whole loading history of all the specimens even though the maximum strain amplitude was as large as 4%.

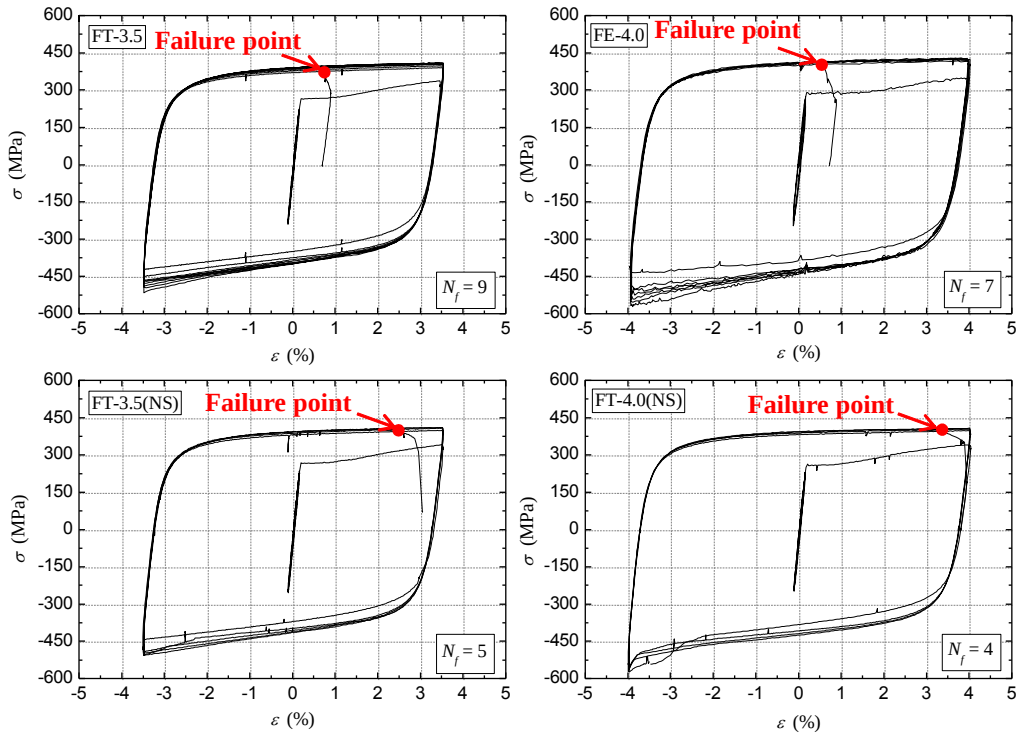

Figure 6: Stress-strain relations.

It is shown in the hysteretic curve of the FT-3.5 specimen with the constant strain amplitude that the first loop is hardly affected by the strain hardening effect while the others are remarkably influenced by the strain hardening effect. At the last loop, the strength decreases rapidly in the tensile state of the BM and then unloading is applied when the axial force fells down by over 10% of the maximum axial force. The same results can be observed in other specimens with the constant strain amplitude.

Hysteretic behaviors of BRB's specimens are unsymmetric in tension and compression, and the maximum absolute compressive stress is 21% to 37% larger than the maximum tensile stress. The reason for this behavior is explained as follows: with the strain amplitude increasing in the compressive state, the contact force and the friction between RMs and the BM increased under the multi-wave deformation.

As listed in Table 4, the failure cycle number N_f of the FT-3.5 specimen with the stopper under the same 3.5% strain amplitude decreased from 9 to 5 in contrast with the FT-3.5(NS) specimen without the stopper, while N_f of the FE-4.0 specimen with the stopper under the same 4.0% strain amplitude decreased from 7 to 4 in contrast with the FT-4.0(NS) specimen without the stopper. It is concluded that the stopper used to prevent the relative displacement obviously affects the low-cycle fatigue performance of steel BRBs.

3.2 Failure mode

Failure modes of the BMs are presented in Figure 7, while failure positions of all the test specimens are sketched out in Figure 7(e). It is clear that crack initiating from the mid-span of the BMs induced the failure of specimens. From the failure modes of the FT-3.5 and FE-4.0 specimens with the stoppers, crack began to appear on the side of the BM and propagate in the transversal direction, but from the failure modes of the FT-3.5(NS) and FT-4.0(NS) specimens without the stoppers, crack began to develop in the middle of the BM and the fold deformations were observed after the failure of the BRB's specimens. So, it is concluded that the stoppers have a noticeable impact on the failure of the BRB, and then the analytical models are proposed to simulate the behaviors of the BRB with or without the stoppers.

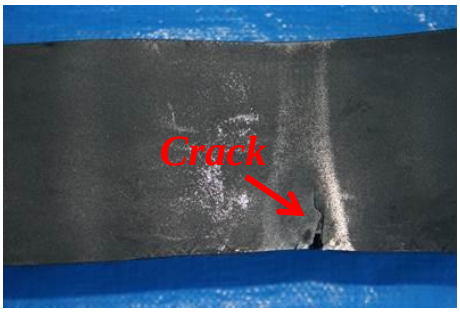

(a) FT-3.5

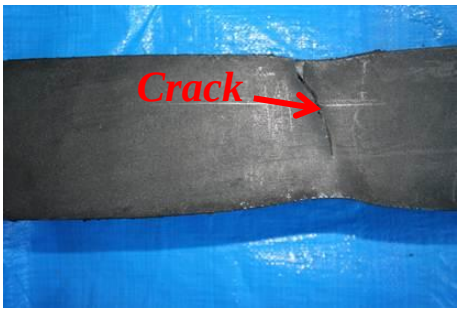

(b) FT-3.5(NS)

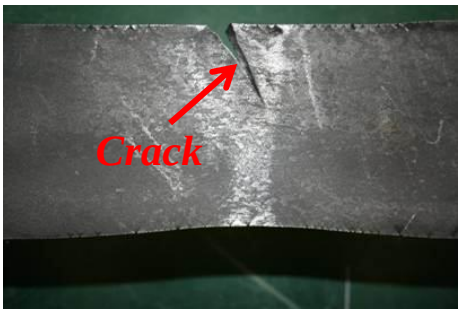

(c) FE-4.0

(d) FT-4.0(NS)

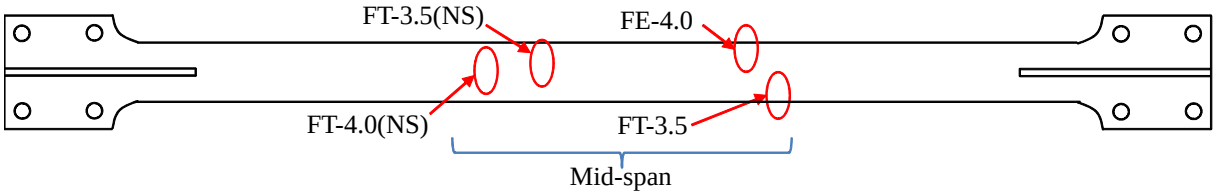

(e) Failure position.

Figure 7: Failure modes of BRB's specimens

3.3 Cumulative inelastic deformation

A measure used in practice to describe the plastic demand on a BRB element is the cumulative inelastic strain, or alternatively, the cumulative inelastic deformation (*CID*). The *CID*, which is expression of the cumulative plastic deformation, is defined by

$$CID = \sum_i \Delta\beta_p^i \tag{1}$$

where, $\Delta\varepsilon_p^i$ = plastic strain during each visit i into the inelastic range, as shown in Figure 8.

The *CID* values of all test specimens are summarized in Table 4. The calculation of the *CID* was achieved with an algorithm that detects local peaks and valleys in the strain history. *CID* values indicate that the *CID* performance of steel BRBs with the stoppers even under the strain amplitude, larger than 3%, can meet the requirements of high-performance BRBs but *CID* performance of steel BRBs without the stoppers cannot meet the requirements of high-performance BRBs.

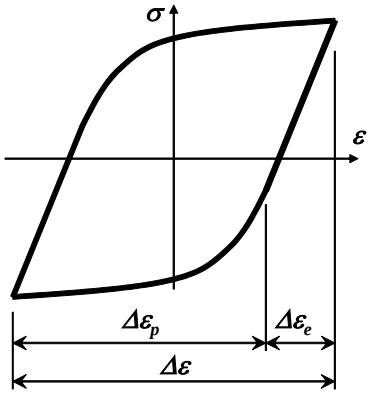

Figure 8: Stress-strain loop.

4 PROPOSED MODELS

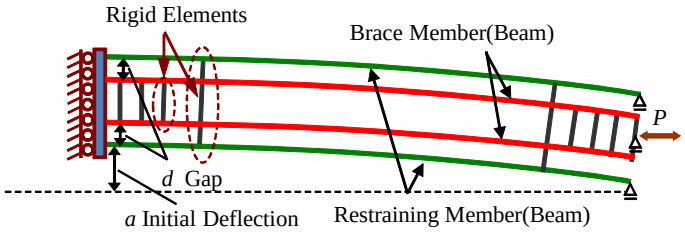

(a) *Half Model*

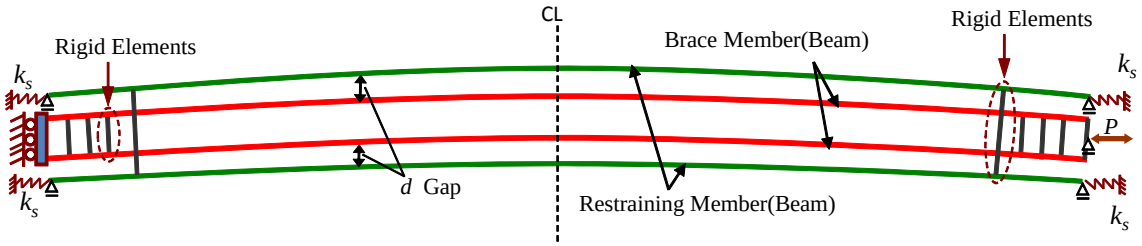

(b) *Whole Model*

Figure 9: Analytical models based on beam element.

In order to simulate the mechanical behaviors of the BRBs with or without stoppers, two analytical models built in ABAQUS[12] are given as follows.

Considering that stoppers are welded on the BM, the mechanical behavior of the BRB is symmetric. So an elastic-plastic 2D model simulating the BRB with the stoppers is proposed and illustrated in Figure 9(a), where half a BRB is modeled under the symmetry condition. A pair of RMs is simulated as two 2D beams equably divided into 54 segments and the BM is also simulated using two 2D beams considering that it is easy to accurately simulate the contact between the BM and RMs. A number of rigid elements between the BM beams are used

to satisfy the linear plane assumption. The same elements are applied between the RMs to simulate high-strength bolts. Initial deflection of a sinusoidal pattern is considered with the maximum value of a, which is set to one thousandth of the length of the BM without cruciform part. The constant gap d between the RMs and the BM is assumed.

The unbonding material was stuck to the BM as the isolation material in order to reduce the friction between the BM and RMs. So, the rigidity of the unbonding material is neglected in this model. However, when one of the BM beams comes into contact with a RM beam, friction effects will exist between them. As shown in Fig. 6, the compressive force is over 20% larger than the tensile force, and therefore the static friction coefficient μ is considered in the model.

Moreover, the horizontal displacement and the rotation are restrained at the mid-span nodes due to symmetry conditions, the vertical displacement is restrained at the right end nodes and the rotation is restrained at the BM's end where the force is applied. A general purpose finite element analysis software ABAQUS is used with 2D Timoshenko beam element (B21) considering shear deformation[12]. The modified two surface model developed by the authors [13] is used for the constitutive law in the analysis.

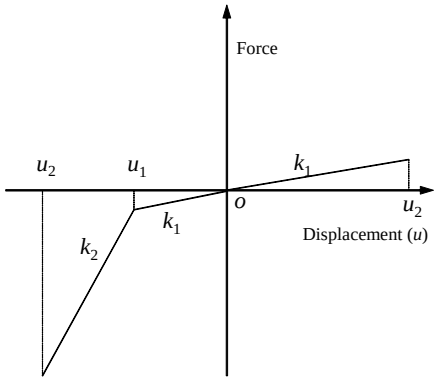

Figure 9: Nonlinear spring force-relative displacement relation.

Because the stoppers were not welded in the FT-3.5(NS) and FT-4.0(NS) specimens' tests, the RMs of the steel BRB, were driven by the friction at the beginning of low-cycle fatigue tests, and were stopped because of the interaction between the RMs and the cruciform section part of the BM in the axial direction. Therefore, the second elastic-plastic model of a whole BRB is presented in Figure 9(b) and the different boundary conditions of the RMs are given. The four nonlinear springs are used to simulate this movement and the force-relative displacement relation of nonlinear springs is given in Figure 9. As shown in Figure 9, the nonlinear spring behavior is defined by a group of the stiffness coefficient and the displacement. The value of k_1, about one thousandth of the axial stiffness of the RM, makes the RM free and the value of k_2, equal to the axial stiffness of the RM, prevents the RM's movement. The displacement u_1 is decided by the gap between the RM and the cruciform section part of the BM, so u_1 is set to 32.5mm. The elements, initial deflection, friction coefficient and material constants are same to the first elastic-plastic model. In order to compare with each other conveniently, the first model is called *Half Model*, and the second model is called *Whole Model*.

5 COMPARISON WITH TEST RESULTS

5.1 Experimental data

In this section, low-cycle fatigue test results of the FT-3.5 and FT-3.5(NS) specimens will be conducted to evaluate the proposed analytical models. As shown in Figure 10, the maximum absolute compressive stress at the first loop of the FT-3.5(NS) specimen is about 5% larger than the FT-3.5 specimen, but it is nearly the same as the FT-3.5 specimen. It is considered that the difference of the first loop is affected by the constraint of the RM. However, the indifference of the last loop is considered to affect by two factors: one is that the stoppers of the FT-3.5 specimen had broken at last, and another is that the residual deformation of the previous loops had an effect on the last loop. So in the next section, we will only use the data of the first loop as the criteria to check the analytical results.

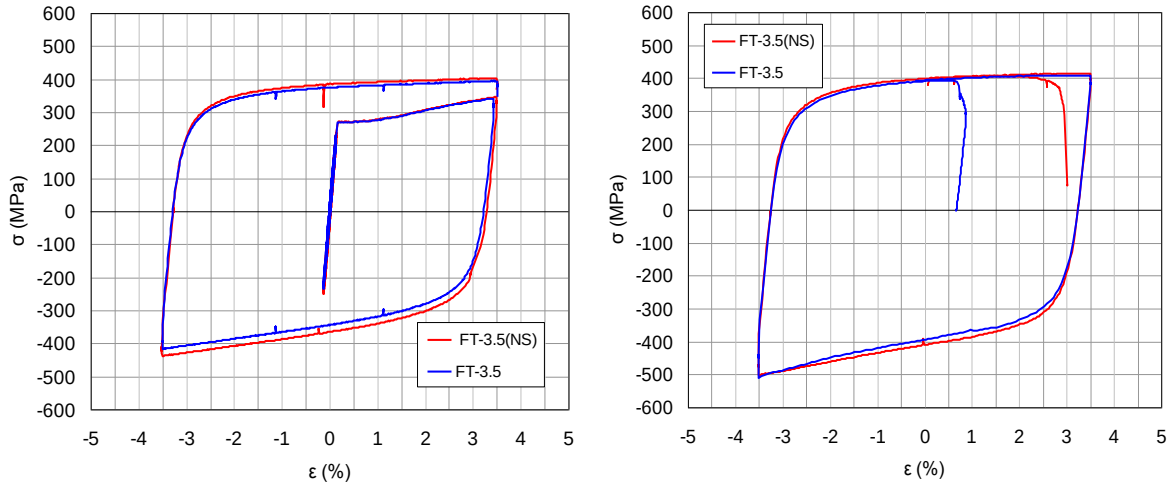

(a) First loop (b) Last loop

Figure 10: Stress-strain relations (μ=0.0).

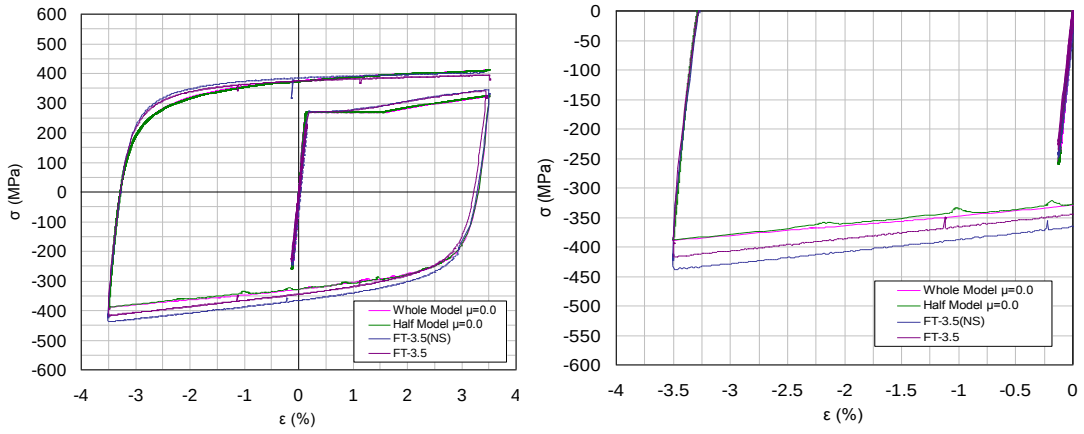

(a) Overall view (b) Partial view

Figure 11: Stress-strain relations (μ=0.0).

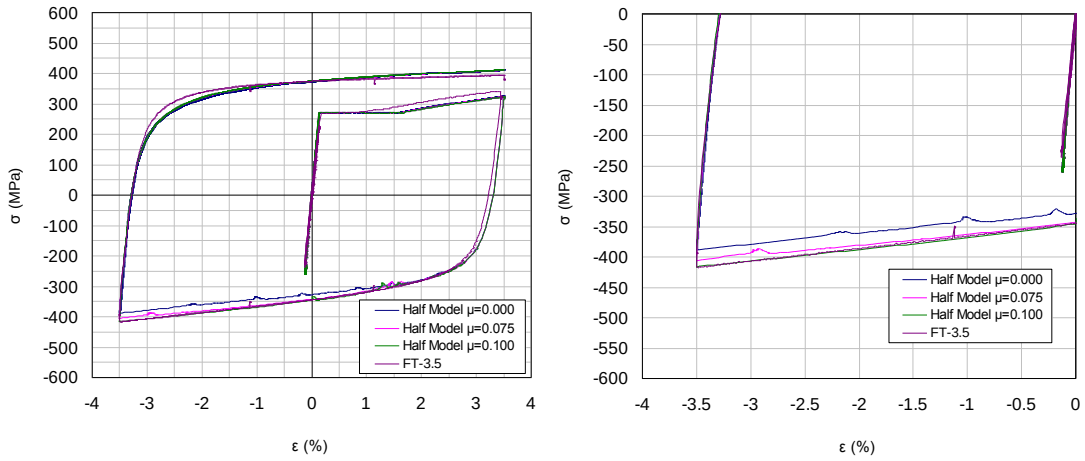

(a) Overall view (b) Partial view

Figure 12: Stress-strain relations of *Half Models* (μ=0.0, 0.075, 0.1).

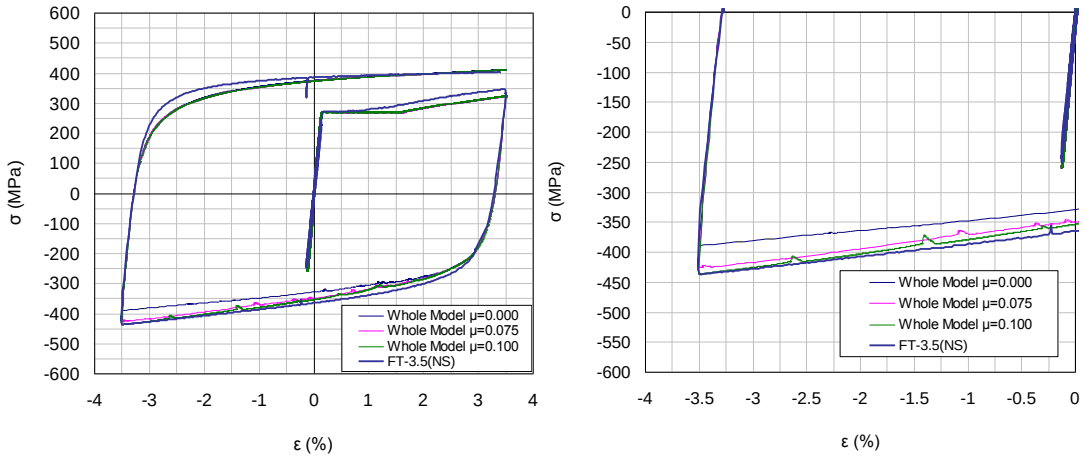

(a) Overall view (b) Partial view

Figure 13: Stress-strain relations of *Whole Models* (μ=0.0, 0.075, 0.1).

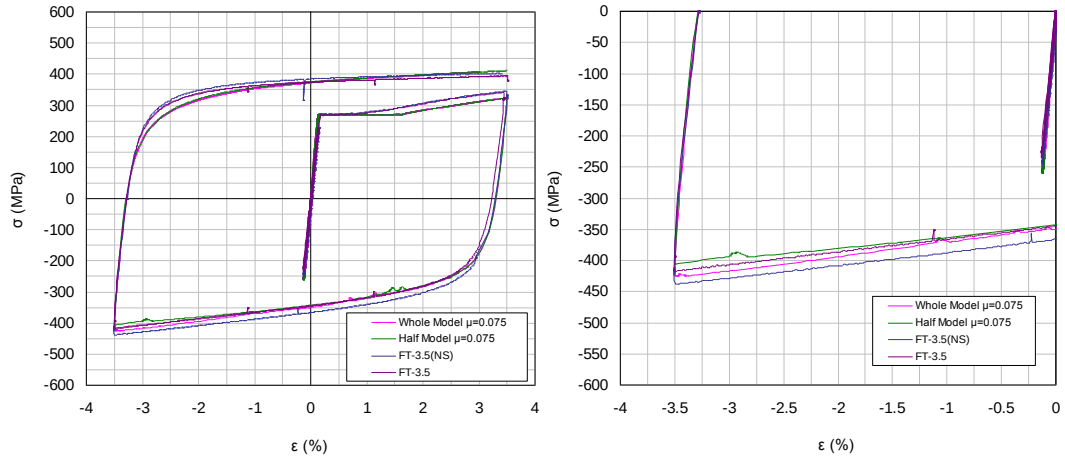

(a) Overall view (b) Partial view

Figure 14: Stress-strain relations (μ=0.075).

5.2 Stress-strain relation

Stress-strain relations of *Half Model* and *Whole Model* are given together with the experimental data in Figure 11. Stress-strain relations of two analytical models are identical and symmetric in tension and compression when the friction between the BMs and the RM is neglected. However, the maximum absolute compressive stress of the first loop of the FT-3.5(NS) specimen is about 13% larger than the results of *Half Model* or *Whole Model*. It can be seen that if the friction is neglected in the analytical model, *Half Model* and *Whole Model* cannot simulate the experiment accurately, but from nearly the same hysteretic behavior, *Half Model* and *Whole Model* are proper.

Stress-strain relations of *Half Model* and *Whole Model* with different friction coefficients are given together with the experimental data in Figures 12 and 13. It is clear that with the friction coefficient increasing, *Half Model* and *Whole Model* can effectively simulate the mechanical behavior of the FT-3.5 and FT-3.5(NS) specimens. As shown in Figure 14, the friction coefficient of 0.075 is regarded as the right value for the following simulations.

5.3 Deformation of BM

The BM's deformations of *Half Model* and *Whole Model* with the same 3.5% compressive strain amplitude are compared in Figure 15. The multi-wave deformation of the *Half Model* is symmetric because of the symmetry conditions. It can be seen that the BM of *Half Model* has fifteen peaks and fifteen valleys, while the BM of *Whole Model* has seventeen peaks and seventeen valleys. So, some of wave peaks of *Whole Model* is sharper than the peaks of *Half Model*. It is considered to be one of the reasons why the failure life of the FT-3.5(NS) specimen is shorter than the failure life of the FT-3.5 specimen.

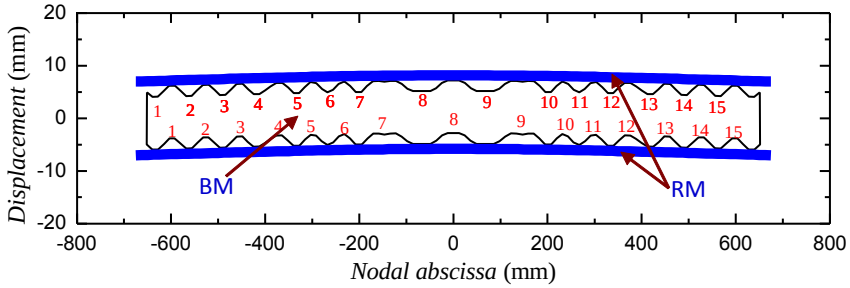

(a) *Half Model*

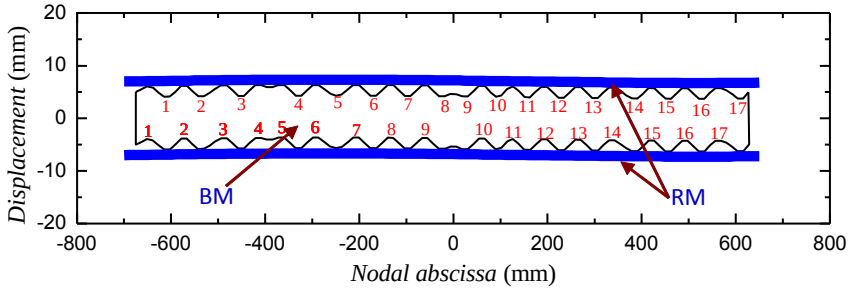

(b) *Whole Model*

Figure 15: Deformation of brace member.

6 CONCLUSION

In this study, low-cycle fatigue tests of benchmark specimens with or without the stoppers were carried out to evaluate the proposed analytical models. The main results are summarized as follows:

1) Low-cycle fatigue tests were conducted to verify that the BRB's specimens with the stoppers possess better low-cycle fatigue performance than the specimens without the stoppers.

2) It was experimentally indicated that the *CID* performance of steel BRBs with the stoppers even under the strain amplitude, larger than 3%, can meet the requirements of HPBRBs but the *CID* performance of steel BRBs without the stoppers cannot meet the requirements of HPBRBs.

3) It is clear that the friction coefficient of 0.075 is regarded as the right value for the simulations and *Half Model* and *Whole Model* can effectively simulate the mechanical behavior of the BRB with or without the stoppers.

REFERENCES

[1] M. Iwata, M. Murai. Buckling-restrained brace using steel mortar planks; performance evaluation as a hysteretic damper. *Earthquake Engineering & Structural Dynamics*, **35**, 1807-1826, 2006.

[2] L.A. Fahnestock, J.M. Ricles, R. Sause. Experimental evaluation of a large-scale buckling-restrained braced frame. *Journal of Structural Engineering (ASCE)*, **133**, 1205-1214, 2007.

[3] T. Usami, Z.H. Lu, H.B. Ge. A seismic upgrading method for steel arch bridges using buckling-restrained braces. *Earthquake Engineering & Structural Dynamics*, **34**, 471-496, 2005.

[4] C.C. Chou, S.Y. Chen. Subassemblage tests and finite element analyses of sandwiched buckling-restrained braces. *Engineering Structures*, **32**, 2108-2121, 2010.

[5] H. Nakamura, T. Takeuchi, Y. Maeda *et al.* Fatigue properties of practical-scale unbonded braces. *Nippon Steel Technical Report*, 2000.

[6] AISC, 2005. Seismic provisions for structural steel buildings, Chicago, Illinois.

[7] T. Usami, H.B. Ge, A. Kasai. Overall buckling prevention condition of buckling-restrained braces as a structural control damper. *Proceedings of the 14th World Conference on Earthquake Engineering*, Beijing, China, 2008.

[8] T. Usami. Developing high-performance damage control seismic dampers. *Proceedings of the 10th symposium on ductile design method for bridges (Special Lecture)*, Tokyo, Japan, 2007.

[9] T. Usami, T. Sato. Low-cycle fatigue tests and verification method for a steel buckling-restrained brace. *Journal of Structural Engineering, JSCE*, **56A**, 486-498, 2010(in Japanese).

[10] T. Usami, C.L. Wang, J. Funayama. Low-cycle fatigue tests of a type of buckling restrained braces. *Proceedings of 12th East Asia-Pacific Conference on Structural Engineering and Construction*, HongKong, 2011.

[11] J. Funayama, C.L. Wang, T. Usami. Improving low-cycle fatigue performance of a type of steel brbs by weld toe-finishing. *Journal of Structural Engineering, JSCE*, **57A**, (in Japanese), 2011.

[12] ABAQUS, 2008. Analysis user's manual(version 6.8). ABAQUS Inc., Pawtucket, R.I.

[13] C. Shen, I. Mamaghani, E. Mizuno *et al.* Cyclic behavior of structural steels. Ii: Theory. *Journal of Engineering Mechanics*, **121**, 1165-1172, 1995.